

Polarization Mechanism Underlying Strongly Enhanced Dielectric Permittivity in Polymer Composites with Conductive Fillers

Bo Li,* Clive A. Randall, and Evangelos Manias*



Cite This: *J. Phys. Chem. C* 2022, 126, 7596–7604



Read Online

ACCESS |



Metrics & More

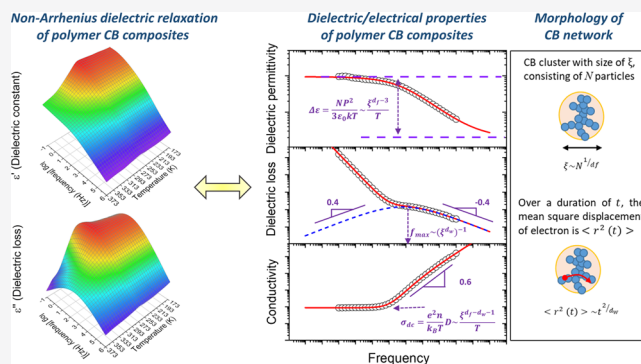


Article Recommendations



Supporting Information

ABSTRACT: Polymer composites filled with conductive fillers can demonstrate ultrahigh effective dielectric permittivity, which is generally attributed to an enhanced Maxwell–Wagner–Sillars interfacial polarization associated with the formation of microcapacitor networks. Here, we explore a composite of the ethylene–propylene–diene elastomer with carbon-black (CB) nanofillers and investigate its dielectric response over wide ranges of temperature and frequency. The dielectric relaxation exhibits atypical (counter-Arrhenius) temperature dependence, contradicting the widely assumed interfacial polarization mechanisms. It is shown that the relaxation/polarization is actually determined by electron displacement—primarily via e-conduction and tunneling within CB clusters—and that the composites' dielectric response can be quantitatively correlated with the CB cluster morphology via a set of scaling laws. Considering the selected composite as a paradigmatic system, the physical origins of the dielectric relaxation and the associated scaling relations seem to be generally applicable and expected to also pertain to other dielectric polymer/conductive-filler composites near percolation.



INTRODUCTION

Ever-increasing challenges in excessive burning of fossil fuels and global climate changes call for solutions to improve energy storage and conversion efficiency, where high- k dielectric materials play a critical role. Polymer composites filled with conductive fillers exhibit a dramatic change in dielectric and electrical properties when filler clusters increase in size and, even more so, when the filler concentration is approaching, but remains below, the percolation threshold.^{1–3} Such materials possess considerable potential for applications as dielectrics—including in charge storage capacitors, high- k gate dielectrics, electromagnetic interference shielding, and electroactive materials—capitalizing on the high dielectric permittivity that can be achieved (ϵ' up to 10^3 to 10^4).^{4–7} It is typically assumed that the substantial increase in dielectric permittivity is associated with the formation of microcapacitor networks, with each microcapacitor consisting of conductive fillers as electrodes separated by polymers in between as dielectric.^{1,8–12} Near percolation, the conductive fillers come very close to but not yet in direct (electrical) contact with each other; consequently, the local electric fields in the filler gaps (occupied by the polymer) become significantly intensified through the charge carriers' migration to and accumulation at the filler–polymer interfaces (cf. microcapacitor charges). This interfacial polarization, typically modeled as a Maxwell–Wagner–Sillars (MWS) relaxation, is generally suggested as responsible for the high values of effective dielectric

permittivity in such dielectric composites with conductive (nano)fillers.

Despite the success of this approach in describing certain behaviors of multiple materials, there are many instances where there exist discrepancies. One characteristic example is observed in research efforts aiming to mitigate dielectric loss by employing core–shell structured fillers:^{13–16} In the case of self-passivated aluminum particles, for example, the formation of an insulating Al_2O_3 shell around the conductive Al core can substantially reduce the dielectric loss of the corresponding polymer composites, but it does so at the expense of the dielectric permittivity.¹⁵ This ϵ' reduction is at odds with the microcapacitor model, which would advocate the same or slightly higher ϵ' values: considering that the surface-passivation did not affect the filler/capacitor distribution and the Al_2O_3 shells were nanometer-thin, the microcapacitor network remained largely unaltered (the conductive Al cores still serving as electrodes while the polymer plus the thin Al_2O_3 shell, both with a similar low dielectric constant, as dielectrics). Another example where the microcapacitor model seems

Received: March 6, 2022

Revised: April 10, 2022

Published: April 25, 2022

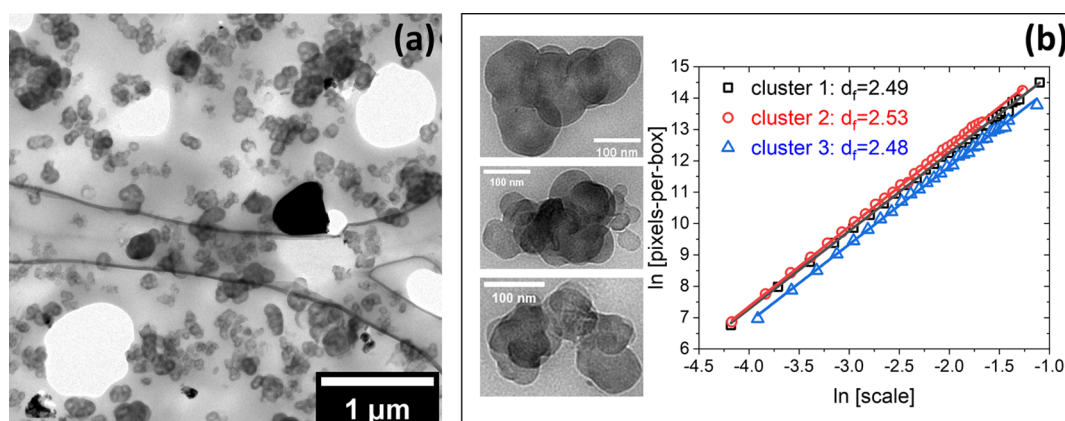


Figure 1. (a) Low magnification TEM image of the CB polymer composite. (b) High mag TEM images of three typical CB clusters and the corresponding derivation of their fractal dimension using the pixel-counting algorithm.

problematic relates to dual-filler polymer composites, whose dielectric response (ϵ' and $\tan \delta$) is found to depend on whether the mesoscopic conductive network is interrupted^{17–20} but is independent of the microcapacitor network. This behavior is contrary to the MWS expectation of larger domain polarization, originating from an increase in space charge populations (e.g., additional surfactants and ions associated with the co-fillers) within a given microcapacitor network geometry.

These experimental results emphasize the importance of electron transport, which is ignored in the microcapacitor and the interfacial polarization models.^{21,22} Here, in order to elucidate the underlying mechanisms in such systems, we investigate the dielectric response (ϵ^* over a broad temperature and frequency range) for a near-percolation carbon black (CB) composite, exhibiting substantial filler clustering: We specifically focus on one particular case [32 wt % CB in an ethylene–propylene–diene (EPDM) matrix,²³ which provides a relaxation process with a strikingly atypical temperature dependence—with relaxation time and magnitude initially increasing and subsequently decreasing with temperature—at odds with normal thermally activated mechanisms, such as Arrhenius processes or MWS polarization. EPDM has many applications due to its excellent resistance to ozone, oxidants, severe weather conditions, oxidation, chemical and heat resistance, and mechanical and dielectric qualities. EPDM composites filled with conductive fillers or high- k ceramic fillers are commonly employed in high-voltage cable splice and termination applications as they can provide internal e-field stress grading, moisture barriers, and mechanical flexibility in addition to outstanding insulating properties.

METHODS

Materials and Sample Preparation. The composite samples are based on a common thermoset olefin elastomer (crosslinkable ethylene propylene diene polymer, EPDM) and CB, with systematically varied CB content (from 15 to 32 wt %). Composites were prepared by mixing the EPDM matrix and CB particles [the EPDM matrix consists of crosslinkable EPDM, a plasticizer (paraffin oil) fixed at a constant relative concentration (30 phr, parts per hundred EPDM rubber), and a fixed relative concentration of peroxide curing agent (dicumylperoxide, DCP, fixed at 5 phr)]. All materials are introduced in one shot inside a lab-scale twin-head kneader (Haake Rheocord 9000). The ratios of the plasticizer and the

curing agent to EPDM were kept constant to ensure the same polymer matrix composition across all composites. Prior to compounding, all materials were dried overnight at 80 °C under a low vacuum. The twin-head kneader was operated at 160 °C for 15 min at low shear rates, $70 < \text{rpm} < 100$. The mixed composites were subsequently cured (hot-pressed) at 170 °C for 10 min and then further cured at 20 °C for 24 h toward 3 mm-thick crosslinked plate-specimens (150–200 cm² in lateral dimensions).

DCP (329541, Sigma-Aldrich) was purchased from Sigma-Aldrich. Paraffin oil (S894, J.T. Baker) was purchased from Fisher Scientific. CB (Spheron 6000, Cabot) and EPDM (Vistalon S420, ExxonMobil Chemical) were provided by Eaton-Cooper. Spheron 6000 was a low structure grade CB with an iodine value of 20 and a DBP value of 92. In each composite, 5 vol % barium titanate (BT-04, Sakai Chemical Industries) was added to improve the high-voltage tracking resistance, stabilize the CB dispersion, and adjust the mechanical properties.

Characterization. For the TEM measurement, thin sections were sectioned from epoxy-embedded samples using a Leica Ultracut UCT Microtome with a cryo-attachment and imaged using a transmission electron microscope (Jeol JEM-2010 with LaB₆ emitter) operated at an accelerating voltage of 200 kV.

The fractal analysis of CB clusters was performed using the Image-J software with the FracLac plugin. TEM digital images were first processed into a grayscale format, and the fractal dimension was calculated by the pixel-counting algorithm. In the grayscale analysis, objects exist in a pseudo-3D plane, and a pixel takes a value between 0 and 255, which scales with the object volume. Unlike the binary analysis where a pixel is either on or off, the grayscale analysis provides a way to measure texture in 3D space by considering the overlapping effect. For the pixel-counting algorithm, grids with varying numbers of boxes were overlaid on the image and the average number of pixels in each box was counted as pixels-per-box (PpB). Data were plotted as $\ln(\text{PpB})$ versus $\ln(\text{box-size})$, the slope of which represented the fractal dimension of the object. The process is shown in Figure S3.

A small-angle X-ray scattering (SAXS) experiment was done using a Xenocs Xeuss 2.0 instrument equipped with a Pilatus 2D detector with a sample-to-detector distance of 1.2 m, using Cu K α radiation ($\lambda = 0.154$ nm) from an X-ray microsource operating at 50 kV and 0.6 mA. The X-ray beam was directed

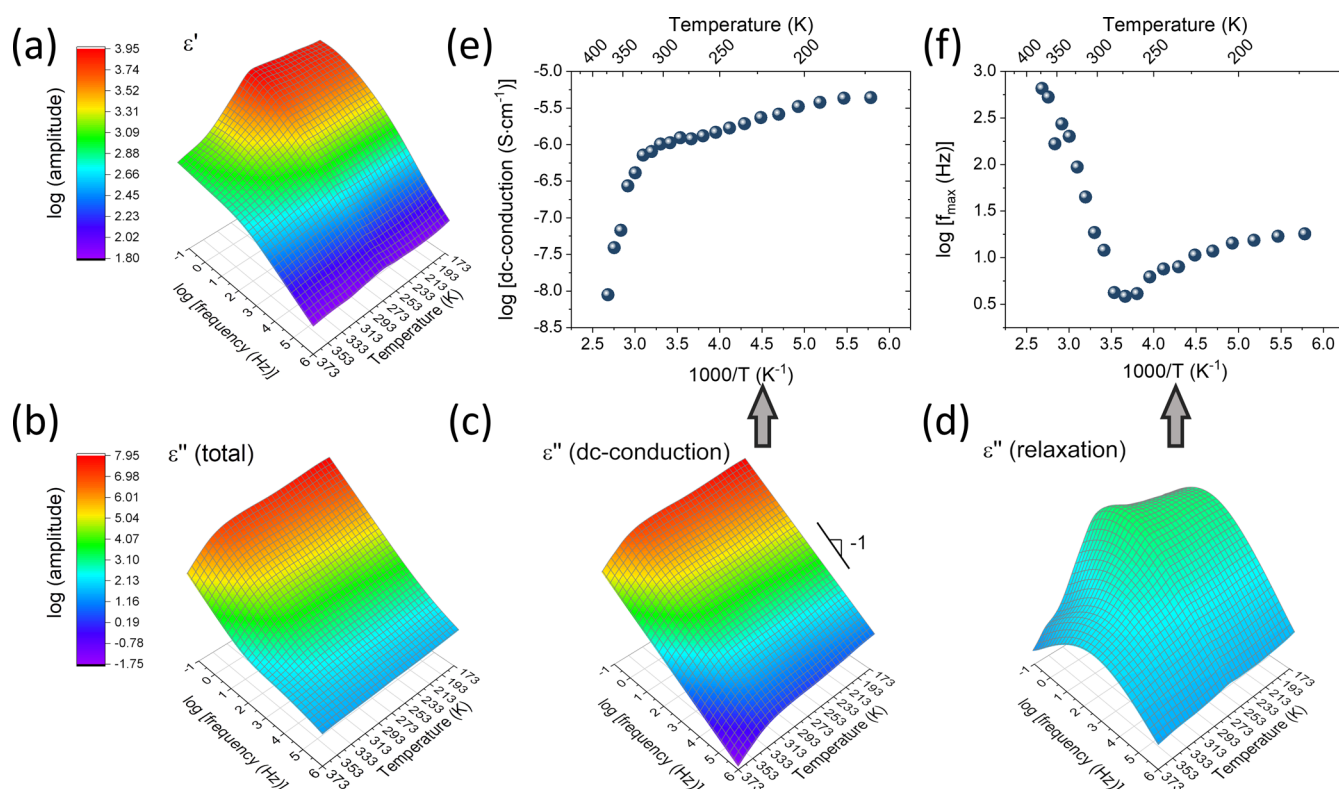


Figure 2. (a,b) Measured dielectric response as a function of temperature and frequency. (c) Conductivity term, assuming the normal w^{-1} scaling for dc conduction. (d) Conduction-corrected dielectric loss, highlighting the dielectric relaxation peak. Arrhenius-temperature plots of (e) conductivity, and (f) relaxation frequency, revealing an atypical, non-thermally activated, non-Arrhenius polarization mechanism.

perpendicular to the surface of a thin layer cut from the bulk sample, and the data acquisition time was 10 min. The one-dimensional SAXS curve was obtained by radial integration of the corresponding 2D pattern using the Foxtrot software.

Dielectric spectroscopy measurement was conducted with a Solartron Modulab MTS test system and a temperature-controlled chamber Delta 9023. The measurement was performed over broad frequency (0.1 to 10^6 Hz) and temperature (-100 to 100 °C) ranges. Before the measurement, 4 cm^2 colloidal silver electrodes ($4 \times 1\text{ cm}$) were painted on both sides of the ca. 3 mm thick samples.

RESULTS AND DISCUSSION

The dielectric properties of the series of EPDM/CB composites (with systematically varied CB concentrations) are shown in Figure S1. The composite containing 32 wt % CB is located well within the sharp transition region where an abrupt increase in the dielectric permittivity is accompanied by enhanced dielectric loss. Figure 1a demonstrates the composite structure. Individual CB particles with an average size of 100 nm are clustered into CB aggregates, which are well-distributed across the entire composite sample. CB particles in the aggregates are separated by nanometer-thin immobilized bound polymer layers,²⁴ and the arrangement of CB can be described by a fractal dimension (d_f)^{2,25}

$$N(r) \sim r^{d_f} \quad (1)$$

where r is the size of the cluster containing $N(r)$ number of CB nanoparticles. For the EPDM/CB composites in question, the fractal dimension of the CB clusters could not be measured by SAXS due to the low angle limit of our instruments (Figure

S2),^{26,27} and instead, the fractal-box method (pixel-counting algorithm) from direct imaging was applied to estimate its value (Figure S3).^{28–30} Specifically, grids with varying mesh sizes are overlaid on TEM images containing single CB clusters, the average number of PpB is enumerated, and the fractal dimension of each CB cluster is calculated from the $\ln(\text{PpB})$ versus $\ln(\text{box size})$ plot, as shown in Figure 1b. As expected, the various CB clusters in the same composite all show a very similar fractal dimension, namely, $d_f \cong 2.5$. The large d_f value indicates a compact cluster structure (the higher the d_f the denser the structure), which is consistent with the low structure grade of the CB used in this study and is also consistent with the classical lattice theory for randomly dispersed occupied sites.^{31,32} The small deviations from the average $d_f = 2.5$ denote a high shape similarity between clusters, suggesting good melt-blending processing (steady-state dispersion) of the CB particles in the largely apolar EPDM matrix.

The temperature- and frequency-dependent dielectric properties of the 32 wt % EPDM/CB composite are shown in Figure 2a,b (with individual frequency scans at each temperature in Figure S4). The dielectric spectra were analyzed within the framework of Cole–Cole plus a conductivity contribution^{33–35} by concurrent fitting of the permittivity and the dielectric loss spectra by

$$\epsilon^*(w) = \epsilon_\infty + \frac{\Delta\epsilon}{1 + (i\omega\tau_R)^{1-\alpha}} + \frac{\sigma_{dc}}{i\omega\epsilon_0} \quad 0 \ll \alpha < 1 \quad (2)$$

where $w = 2\pi f$ is the angular frequency; $\Delta\epsilon = \epsilon_s - \epsilon_\infty$ is the dielectric relaxation strength, with ϵ_s and ϵ_∞ being the low- and high-frequency limits of ϵ' , respectively; τ_R is the relaxation

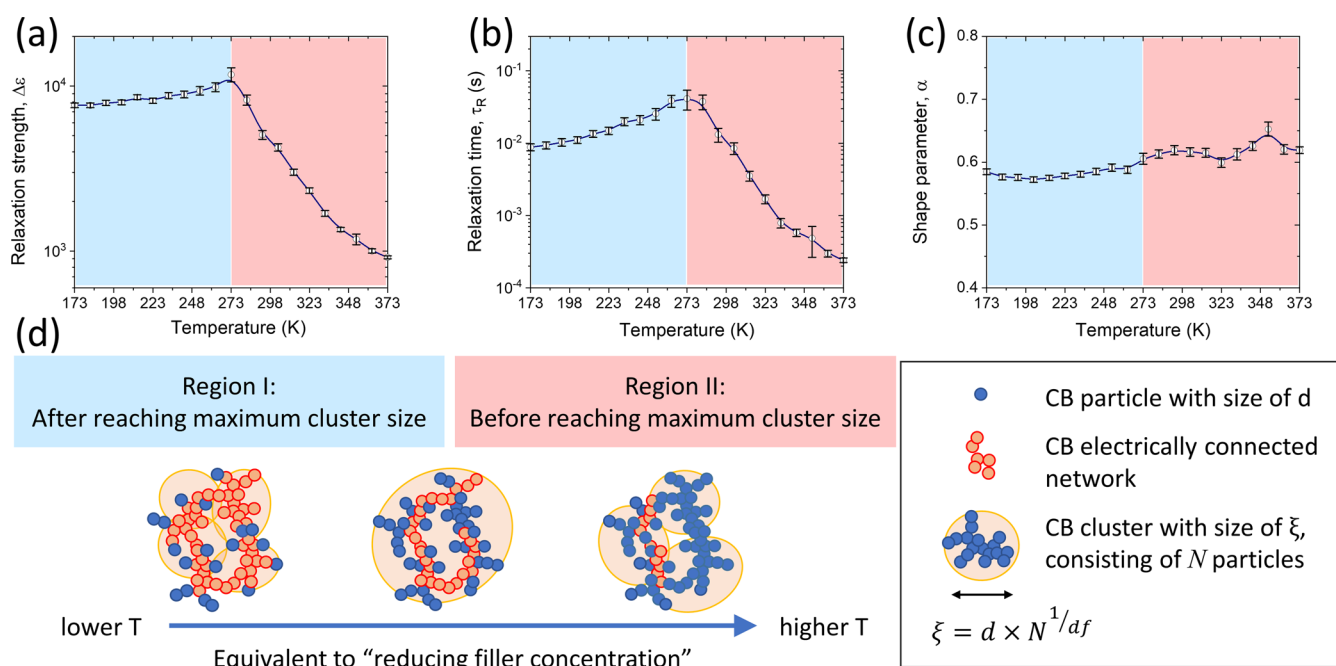


Figure 3. (a–c) Best-fit parameters of the Cole–Cole with experimental temperature; there exist two distinct temperature trends for $\Delta\epsilon$ and τ_R , which are highlighted with different colors across the fitted $\Delta\epsilon(T)$ max. (d) Schematic depiction of the change in cluster “size” with temperature in the two respective regions. The orange circle represents clusters, the size of which increases with reducing temperature until percolation and then decreases afterward. Red CBs are the particles that can form electrically connected pathways across the sample, while blue CBs are those that cannot form the throughgoing network.

time related to the loss peak frequency (f_{\max}), that is, $\tau_R = 1/2\pi f_{\max}$; α is the shape parameter characterizing the slopes of the loss curve at the low- and high-frequency limits with respect to f_{\max} ; σ_{dc} is the DC conductivity; and ϵ_0 is the vacuum permittivity. Assuming a normal diffusion for charge transport at low frequencies,³⁶ that is, conductivity scaling with ω^{-1} , Figure 2c, the conduction loss can be subtracted from Figure 2b, and a definitive dielectric relaxation can be quantified through the ϵ'' loss peak and the associated step-change in the ϵ' dielectric permittivity, Figure 2a,d.

At the outset, it becomes clear that the measured dielectric and electrical behaviors do not follow the typical temperature dependence of thermally activated processes: The dc-conductivity plotted versus temperature, Figure 2e, shows the conductivity decreasing with temperature throughout, whereas the relaxation frequency shows a marked and atypical decrease with temperature in the lower-temperature region, Figure 2f. Both observations challenge the widely assumed MWS polarization mechanism as the application of an Arrhenius equation to these data would have yielded a negative activation energy; but are consistent with e-tunneling between adjacent CB particles.^{37,38} Surprisingly, few prior studies have discussed this atypical (non-thermally activated) mechanism, although reporting quantitatively similar dielectric spectra as the ones shown in Figure 2: In some cases, analyses are limited to composites with lower filler concentrations where the typical Arrhenius-type dielectric responses manifest,^{4,36,39–42} whereas, other studies have reported the ultrahigh permittivity behavior for near-percolated composites but were carried out over narrower temperature ranges where the abnormal behavior is not observed in dielectric relaxation spectroscopy (DRS)^{43–45} (i.e., in the present study, e.g., if the dielectric study were limited to $T > 273$ K, only the Arrhenius-like part of the response would have been recorded, Figure 2f).

The best-fit Cole–Cole parameters are shown in Figure 3a–c. Two different temperature dependences can be identified: in the lower- T region, the relaxation strength and relaxation time increase with temperature; whereas in the higher- T region, both parameters decrease with T , Figure 3a,b; the shape parameter remains nearly constant at $\alpha = 0.6$ throughout, Figure 3c. These non-monotonic temperature trends indicate a rather complex nature for the dielectric relaxation, at odds with common thermally activated processes.

The relaxation strength of the composite has a magnitude of 10^3 to 10^4 for this 32 wt % composite (orders of magnitude higher than the $\Delta\epsilon$ measured for the respective unfilled polymer and for the same composites with less than ca. 25 wt % CB, Figure S1). This clearly indicates a domain polarization process substantially greater than the polarization of the corresponding polymer matrix and of the corresponding CB fillers and polymer/filler interfaces and so on (which do manifest in the lower CB content composites).^{46–48} This excess domain polarization can be attributed to electron displacements, e.g. e-tunneling between adjacent CB particles, within the CB clusters (also amplified by limited electron transport between clusters, when such transport occurs).

For conductive filler clusters under electric fields, electrons will migrate to and accumulate at one end, leaving the other end with more positive charges. This process would establish an effective dipole moment across the fillers. When the electric field is reversed, the opposite occurs. This charging and discharging of conductive fillers is in many respects similar to dipolar orientations as observed in polar materials. Therefore, the electron displacement in conductive fillers underlies the polarization of the conductive fillers.⁴⁶ For individual well-separated CB particles, electrons predominately form dipoles across a single CB particle. With increasing filler concentration, CB particles start to aggregate into clusters, and electrons can

now form dipoles over the whole cluster, with dipole moments determined by the cluster size/length-scale and the electron population from multiple/all CB particles of the cluster (assuming a long enough time for electrons to cross over to neighboring CB particles within the cluster). If this is the case, the composite dielectric properties (Figures 2e,f and 3a,b) are reasonable.

Reducing temperature is equivalent to shrinkage of the EPDM matrix and closer proximity between CB particles or also equivalent to an increasing effective CB concentration. As a result, as schematically shown in Figure 3d, for near-percolated composites, the cluster size (orange circle) will increase with decreasing temperature (c.f., increasing filler concentration) until a percolated filler structure is established (i.e., cluster size reaches the maximum); further reducing the temperature will decrease the cluster size. The divergence of the cluster size across percolation is commonly reported for percolating composites.^{2,21}

The relaxation strength and relaxation time are both expected to scale with cluster size (vide infra eqs 5 and 6), which would also diverge across the percolation. Meanwhile, conductivity will always increase with reducing temperature as more throughgoing conduction pathways are formed (represented by the red CB in Figure 3d).

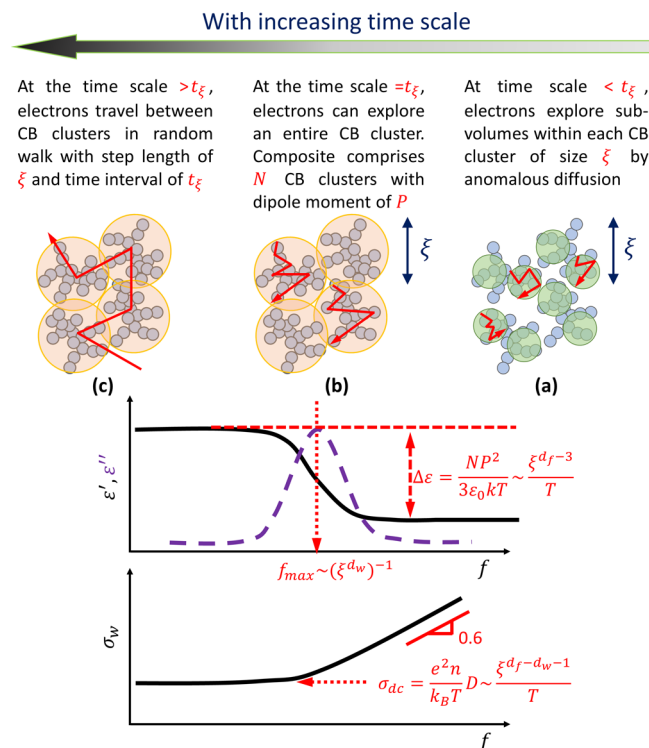
If the electron displacement within CB were the dominant polarization mechanism responsible for the observed dielectric response, one should also be able to derive scaling relations for the dielectric functions with the composite/cluster morphology sizes and with time and subsequently compare the corresponding scalings against the experimentally measured data. While the detailed derivation is provided in the Supporting Information, the most critical correlations are summarized below.

Starting with the conductivity: As depicted in Scheme 1, at high frequencies, electrons only have enough time to move within the CB cluster (where CB particles are arranged into a heterogeneous fractal structure), and these electron movements manifest as an ac conductivity (anomalous diffusion); at low frequencies, sufficiently long times are allowed for electrons to escape the cluster and move within the macroscopic filler network, resulting in a dc conductivity (normal diffusion for a uniform random network of fillers/clusters). Thus, the transition from ac to dc conductivity would occur as the mean electron displacement becomes greater than the cluster size ($r > \xi$) and would correspond to a transition from anomalous diffusion to normal diffusion for the electron transport;^{22,49} the crossover frequency identifies the time scale over which electrons can explore an entire CB cluster. With this understanding, the scaling of conductivity with measurement time can be quantified based on the cluster size and the arrangements of CB inside the clusters, as detailed in the derivation of eq 55

$$\sigma(\omega) \sim \omega^{(d_w - d_f + 1)/d_w} \sim \begin{cases} \omega^{0.605}, & r < \xi \\ \omega^0, & r > \xi \end{cases} \quad (3)$$

$\sigma(\omega)$ is the conductivity measured at the frequency ω ; d_f and d_w are determined by the morphology of the filler arrangement perceived by electrons during the measurement duration. Namely, d_f is the fractal dimension of the CB network (for length scales smaller than the cluster size ξ , d_f is the cluster's fractal dimension of 2.5, Figure 1b, and for longer length scales d_f is simply 3, a homogenous three-dimensional filler network);

Scheme 1. Schematic Illustrating the Electron Transport (Red Arrows) at Different Time Scales and the Corresponding Dielectric and Electrical Behaviors (σ_{dc} Contribution Is Subtracted from the ϵ'' Spectrum for Clarity): (a) At the High-Frequency End, Electrons Are Confined within a Filler Cluster and Follow Anomalous Diffusion, Exhibiting an ac Conductivity^a



^aWith an increasing measurement time duration, the polarizable domain (green circle) is growing, accounting for an increase in the dielectric constant. (b) The growth of the polarizable domain ceases when it approaches the cluster size (orange circle), manifested as the leveling off of the dielectric constant. (c) Further increasing the measurement duration will enable inter-cluster electron transport (long-range normal diffusion) and give rise to a dc conductivity while leaving the dielectric constant unaltered.

d_w is the diffusion exponent describing the scaling between mean-square electron displacement and time, which assumes a value of 2 for normal diffusion (electron transport between clusters) and 3.8 for anomalous diffusion (electron transport within a cluster).^{25,32}

In eq 3, the derived scaling exponent of the high-frequency conductivity, 0.605, is very close to the shape parameter (α) measured from the experimental data (Figure 3c). As defined in eq 2 and shown in Figure S5, α characterizes the slope of the loss (ϵ'') curve of dielectric relaxation and would also equate to the slope of the conductivity at the high-frequency end, as $\sigma(\omega) = \omega \epsilon_0 \epsilon''$. A consistent α value of ~ 0.6 measured across the whole temperature range confirms the electron displacement within CB clusters as the dominant polarization mechanism in the CB polymer composite.

The same scalings (d_f , d_w) also define the low-frequency conductivity (σ_{dc}), which is proportional to the population of mobile charges (electrons)—that is, the electron density within CB clusters ($n \sim N(\xi)/\xi^3 \sim \xi^{d_f}/\xi^3$)—and their mobility D —that is, electrons exploring the cluster size ξ

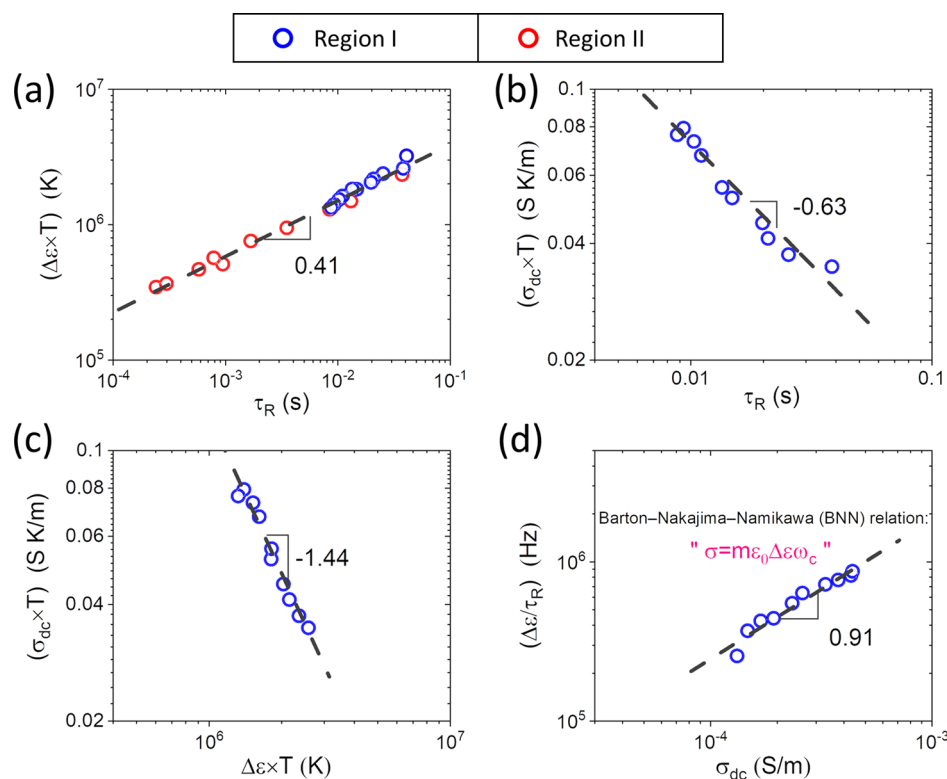


Figure 4. Experimental relations between dielectric properties. The number on the graphs represents the slope of the linear regression from the DRS experimental data, which is in good agreement with the scaling predictions (eqs 7 and 8).

over a time interval $t_{\xi} \sim \xi^{d_w}$ (Scheme 1). The corresponding scaling of σ_{dc} with ξ is as detailed in the derivation of eq S9

$$\sigma_{dc} \sim \frac{n \cdot D}{T} \sim \frac{1}{T} \left(\frac{\xi^{d_f}}{\xi^3} \cdot \frac{\xi^2}{\xi^{d_w}} \right) \sim \frac{\xi^{d_f - d_w - 1}}{T} = \frac{\xi^{-2.3}}{T} \quad (4)$$

Now considering the dielectric properties: A schematic representation is also shown in Scheme 1, which illustrates how the dielectric properties of the composite relate to the movement of electrons within the polarizable domains (CB cluster network). Over longer time scales, that is, as the measurement frequency is reduced, electrons explore increasingly larger volumes, that is, larger polarizable domains, and yield an associated increase in the dielectric constant (apparent dielectric permittivity). For long enough times, the polarizable domain spans the whole CB cluster (reaches a maximum size), and after that, the electron transport changes from exploring a single CB cluster to moving between clusters (i.e., from anomalous to normal diffusion, a transition from ac to dc conduction, and an associated change from a frequency-dependent dielectric permittivity to a constant value). This is commonly reported for systems where space-charge polarization (in which only sub-diffusive charge motion contributes to the permittivity) changes to normal-diffusive charge motion as the measurement moves to lower frequencies; this later charge mobility is associated with dc conductivity and a constant value dielectric constant.^{34,46}

From the perspective of the above-mentioned cluster polarization, the DRS relaxation strength ($\Delta\epsilon$) quantifies the magnitude of electron displacement within a cluster, whereas the DRS relaxation time (τ_R) quantifies the time needed for electrons to explore the cluster. Both parameters would be

positively correlated with the cluster size (ξ), as detailed in the derivation of eqs S10 and S13

$$\tau_R \sim \xi^{d_w} = \xi^{3.8} \quad (5)$$

$$\Delta\epsilon \sim \frac{\xi^{d_f - 1}}{T} = \frac{\xi^{1.5}}{T} \quad (6)$$

The electron displacement and cluster polarization mechanism are straightforward and intuitive. However, the quantitative scaling relations (eqs 3–6) seem rather ad hoc; fortunately, the direct experimental verification of all scaling relations is enabled by comparing eqs 3–6 to the dielectric spectra (measured by DRS) and the filler cluster morphology (measured by TEM). Namely, by combining eqs 3–6, we can reduce the variable of the cluster size (ξ) and obtain

$$\begin{aligned} \Delta\epsilon \cdot T &\sim \tau_R^{0.40}; & \sigma_{dc} \cdot T &\sim \tau_R^{-0.61}; \\ \sigma_{dc} \cdot T &\sim (\Delta\epsilon \cdot T)^{-1.53} \end{aligned} \quad (7)$$

which provide testable non-trivial inter-relations between various DRS quantities, as shown in Figure 4a–c. A remarkably good agreement with the experimental data is observed, confirming the scaling predictions of eq 7 and of the underlying mechanism described above (eqs 3–6).

Finally, we can also reduce the temperature variable out from eqs 3–6, obtaining:

$$\sigma_{dc} \sim \frac{\xi^{d_f - d_w - 1}}{T} = \frac{\xi^{d_f - 1}}{T} \cdot \xi^{-d_w} \sim \Delta\epsilon \cdot \frac{1}{\tau_R} \quad (8)$$

which is an inter-relation between $\Delta\epsilon$, τ_R and σ_{dc} (also satisfactorily confirmed by the experimental results, as shown in Figure 4d). This last relation connects three of the four

experimental DRS quantities (the fourth being the shape parameter, α) and bears similarity to the phenomenological Barton–Nakajima–Namikawa (BNN) universal law:^{46,50} $\sigma_{dc} = m\varepsilon_0\Delta\varepsilon\cdot w_c$ (m is a constant of order 1, w_c is the peak frequency of dielectric loss, i.e., $w_c \sim 1/\tau_R$). The derivation of eq 8 from the scaling eqs 3–6 reveals hints about the physical origins of the BNN empirical law in the present polymer/CB composites (i.e., a common length scale underlying both the conductivity and the dielectric polarization, in these systems, the size of the fractal filler clusters, suggesting that the same population of charge carriers responsible for the sub-cluster and cluster polarization gives rise to conductivity at longer experimental time scales).

CONCLUSIONS

In this paper, we systematically investigate the temperature and frequency dependence of the dielectric properties for the EPDM-elastomer/CB composite, for a filler concentration close to but lower than the conductive percolation threshold; the primary focus was to understand the physical mechanisms underlying the substantial increase in (apparent) dielectric permittivity. A strong, non-monotonic, non-Arrhenius polarization was recorded, at odds with the widely assumed MWS polarization. It is revealed that this polarization is dominated by the electron displacement within the CB clusters, including e- tunneling, rather than by polarizations occurring at the filler/filler or the filler/polymer interfaces. Scaling relations between the electron transport and the clusters' fractal dimension and size were proposed, and their predictions were compared favorably against the DRS experimental findings. From a practical viewpoint, these materials possess a very promising dielectric response as insulators, if the multi-filler cluster morphology is properly designed, as this study indicates, rather than only modifying the fillers' inherent properties and interfaces. For instance, an enlarged filler cluster is a prerequisite to achieving a high dielectric constant, while blocking electron transport between clusters is the key to reducing dielectric loss, both of which can be realized by introducing a high aspect-ratio insulating co-filler (e.g., nanoclay or boron nitride) in between the clusters of the conductive fillers.

ASSOCIATED CONTENT

Supporting Information

The Supporting Information is available free of charge at <https://pubs.acs.org/doi/10.1021/acs.jpcc.2c01592>.

Dielectric properties of polymer composites with different CB concentrations; small-angle XRD measurement of the CB polymer composite; estimation of the fractal dimension of the CB cluster via the pixel-counting algorithm; deconvolution results of dielectric spectra; correlated dielectric/conductivity spectra; and detailed derivation of scaling relations between dielectric variables (PDF)

AUTHOR INFORMATION

Corresponding Authors

Bo Li – Department of Materials Science and Engineering and Center for Dielectrics and Piezoelectrics (CDP), The Pennsylvania State University, University Park, Pennsylvania 16802, United States; PolyK Technologies, State College,

Pennsylvania 16803, United States; orcid.org/0000-0002-4890-8435; Email: bolipsu@gmail.com

Evangelos Manias – Department of Materials Science and Engineering and Center for Dielectrics and Piezoelectrics (CDP), The Pennsylvania State University, University Park, Pennsylvania 16802, United States; orcid.org/0000-0003-0705-0601; Email: manias@psu.edu

Author

Clive A. Randall – Department of Materials Science and Engineering and Center for Dielectrics and Piezoelectrics (CDP), The Pennsylvania State University, University Park, Pennsylvania 16802, United States

Complete contact information is available at: <https://pubs.acs.org/10.1021/acs.jpcc.2c01592>

Notes

The authors declare no competing financial interest.

ACKNOWLEDGMENTS

This work was supported in part by the National Science Foundation through the “Center for Dielectrics and Piezoelectrics” under NSF grants IIP-1361571 and IIP-1361503, and in part by Eaton-Cooper.

ADDITIONAL NOTE

“The same behavior is also observed for slightly lower filler concentrations (e.g., the 29 wt % CB composite shows qualitatively the same response, albeit with a less pronounced dielectric relaxation, which would introduce more uncertainty in the curve fitting and is not used here for analysis), whereas for composites with much lower CB concentrations (e.g., 20 wt % CB and lower), the dielectric relaxation resumes the usual thermally activated behavior. Therefore, this study strongly suggests that the reported atypical dielectric response is associated with the marked change in dielectric properties, that is, manifestation of ultrahigh dielectric permittivity, and is probably related to, or originates from, electron transport within CB clusters and inter-cluster geometry and separation.

REFERENCES

- (1) Nan, C.-W.; Shen, Y.; Ma, J. Physical Properties of Composites Near Percolation. *Annu. Rev. Mater. Res.* **2010**, *40*, 131–151.
- (2) Stauffer, D.; Aharony, A. *Introduction to Percolation Theory*; Taylor & Francis: London, 1992.
- (3) Dang, Z.-M.; Yuan, J.-K.; Zha, J.-W.; Zhou, T.; Li, S.-T.; Hu, G.-H. Fundamentals, processes and applications of high-permittivity polymer-matrix composites. *Prog. Mater. Sci.* **2012**, *57*, 660–723.
- (4) Wang, B.; Huang, W.; Chi, L.; Al-Hashimi, M.; Marks, T. J.; Facchetti, A. High-k Gate Dielectrics for Emerging Flexible and Stretchable Electronics. *Chem. Rev.* **2018**, *118*, 5690–5754.
- (5) Li, B.; Xidas, P. I.; Manias, E. High Breakdown Strength Polymer Nanocomposites Based on the Synergy of Nanofiller Orientation and Crystal Orientation for Insulation and Dielectric Applications. *ACS Appl. Nano Mater.* **2018**, *1*, 3520–3530.
- (6) Dang, Z.-M.; Yuan, J.-K.; Yao, S.-H.; Liao, R.-J. Flexible Nanodielectric Materials with High Permittivity for Power Energy Storage. *Adv. Mater.* **2013**, *25*, 6334–6365.
- (7) Li, B.; Xidas, P. I.; Triantafyllidis, K. S.; Manias, E. Effect of Crystal Orientation and Nanofiller Alignment on Dielectric Breakdown of Polyethylene/Montmorillonite Nanocomposites. *Appl. Phys. Lett.* **2017**, *111*, 082906.
- (8) He, F.; Lau, S.; Chan, H. L.; Fan, J. High Dielectric Permittivity and Low Percolation Threshold in Nanocomposites Based on

- Poly(vinylidene fluoride) and Exfoliated Graphite Nanoplates. *Adv. Mater.* **2009**, *21*, 710–715.
- (9) Shen, Y.; Lin, Y.; Li, M.; Nan, C.-W. High Dielectric Performance of Polymer Composite Films Induced by a Percolating Interparticle Barrier Layer. *Adv. Mater.* **2007**, *19*, 1418–1422.
- (10) Yousefi, N.; Sun, X.; Lin, X.; Shen, X.; Jia, J.; Zhang, B.; Tang, B.; Chan, M.; Kim, J.-K. Highly Aligned Graphene/Polymer Nanocomposites with Excellent Dielectric Properties for High-Performance Electromagnetic Interference Shielding. *Adv. Mater.* **2014**, *26*, 5480–5487.
- (11) Xia, X.; Wang, Y.; Zhong, Z.; Weng, G. J. A Theory of Electrical Conductivity, Dielectric Constant, and Electromagnetic Interference Shielding for Lightweight Graphene Composite Foams. *J. Appl. Phys.* **2016**, *120*, 085102.
- (12) Wang, L.; Dang, Z.-M. Carbon Nanotube Composites with High Dielectric Constant at Low Percolation Threshold. *Appl. Phys. Lett.* **2005**, *87*, 042903.
- (13) Han, K.; Li, Q.; Chen, Z.; Gadinski, M. R.; Dong, L.; Xiong, C.; Wang, Q. Suppression of energy dissipation and enhancement of breakdown strength in ferroelectric polymer-graphene percolative composites. *J. Mater. Chem. C* **2013**, *1*, 7034–7042.
- (14) Huang, X.; Jiang, P. Core-Shell Structured High-k Polymer Nanocomposites for Energy Storage and Dielectric Applications. *Adv. Mater.* **2015**, *27*, 546–554.
- (15) Xu, J.; Wong, C. P. Low-Loss Percolative Dielectric Composite. *Appl. Phys. Lett.* **2005**, *87*, 082907.
- (16) Zhou, W.; Li, T.; Yuan, M.; Li, B.; Zhong, S.; Li, Z.; Liu, X.; Zhou, J.; Wang, Y.; Cai, H.; Dang, Z.-M. Decoupling of Inter-Particle Polarization and Intra-Particle Polarization in Core-Shell Structured Nanocomposites Towards Improved Dielectric Performance. *Energy Storage Mater.* **2021**, *42*, 1–11.
- (17) Xiao, Y.-j.; Wang, W.-y.; Lin, T.; Chen, X.-j.; Zhang, Y.-t.; Yang, J.-h.; Wang, Y.; Zhou, Z.-w. Largely Enhanced Thermal Conductivity and High Dielectric Constant of Poly(vinylidene fluoride)/Boron Nitride Composites Achieved by Adding a Few Carbon Nanotubes. *J. Phys. Chem. C* **2016**, *120*, 6344–6355.
- (18) Etika, K. C.; Liu, L.; Hess, L. A.; Grunlan, J. C. The Influence of Synergistic Stabilization of Carbon Black and Clay on the Electrical and Mechanical Properties of Epoxy Composites. *Carbon* **2009**, *47*, 3128–3136.
- (19) Konishi, Y.; Cakmak, M. Nanoparticle induced network self-assembly in polymer-carbon black composites. *Polymer* **2006**, *47*, 5371–5391.
- (20) Li, B.; Salcedo-Galan, F.; Xidas, P. I.; Manias, E. Improving Electrical Breakdown Strength of Polymer Nanocomposites by Tailoring Hybrid-Filler Structure for High-Voltage Dielectric Applications. *ACS Appl. Nano Mater.* **2018**, *1*, 4401–4407.
- (21) Pötschke, P.; Dudkin, S. M.; Alig, I. Dielectric Spectroscopy on Melt Processed Polycarbonate—Multiwalled Carbon Nanotube Composites. *Polymer* **2003**, *44*, 5023–5030.
- (22) Gefen, Y.; Aharony, A.; Alexander, S. Anomalous Diffusion on Percolating Clusters. *Phys. Rev. Lett.* **1983**, *50*, 77–80.
- (23) Ryan, D. E.; Manias, E.; Li, B. Elastomer Composites with High Dielectric Constant. US Patent 10438717, Oct. 8, 2019.
- (24) Litvinov, V. M.; Orza, R. A.; Klüppel, M.; van Duin, M.; Magusin, P. C. M. M. Rubber-Filler Interactions and Network Structure in Relation to Stress-Strain Behavior of Vulcanized, Carbon Black Filled EPDM. *Macromolecules* **2011**, *44*, 4887–4900.
- (25) Bunde, A.; Havlin, S. *Fractals and Disordered Systems*; Springer Berlin Heidelberg: Berlin, Heidelberg, 2012.
- (26) Ehrburger-Dolle, F.; Hindermann-Bischoff, M.; Livet, F.; Bley, F.; Rochas, C.; Geissler, E. Anisotropic Ultra-Small-Angle X-ray Scattering in Carbon Black Filled Polymers. *Langmuir* **2001**, *17*, 329–334.
- (27) Koga, T.; Hashimoto, T.; Takenaka, M.; Aizawa, K.; Amino, N.; Nakamura, M.; Yamaguchi, D.; Koizumi, S. New Insight into Hierarchical Structures of Carbon Black Dispersed in Polymer Matrices: A Combined Small-Angle Scattering Study. *Macromolecules* **2008**, *41*, 453–464.
- (28) Captur, G.; Muthurangu, V.; Cook, C.; Flett, A. S.; Wilson, R.; Barison, A.; Sado, D. M.; Anderson, S.; McKenna, W. J.; Mohun, T. J.; Elliott, P. M.; Moon, J. C. Quantification of Left Ventricular Trabeculae Using Fractal Analysis. *J. Cardiovasc. Magn. Reson.* **2013**, *15*, 36.
- (29) Smith, T. G.; Lange, G. D.; Marks, W. B. Fractal methods and results in cellular morphology - dimensions, lacunarity and multifractals. *J. Neurosci. Methods* **1996**, *69*, 123–136.
- (30) Liu, C.; Shi, B.; Zhou, J.; Tang, C. Quantification and Characterization of Microporosity by Image Processing, Geometric Measurement and Statistical Methods: Application on SEM Images of Clay Materials. *Appl. Clay Sci.* **2011**, *54*, 97–106.
- (31) Bunde, A.; Kantelhardt, J. W. Diffusion and Conduction in Percolation Systems. In *Diffusion in Condensed Matter: Methods, Materials, Models*; Heijmans, P., Kärger, J., Eds.; Springer Berlin Heidelberg: Berlin, Heidelberg, 2005, pp 895–914.
- (32) Clerc, J. P.; Giraud, G.; Laugier, J. M.; Luck, J. M. The Electrical Conductivity of Binary Disordered Systems, Percolation Clusters, Fractals and Related Models. *Adv. Phys.* **1990**, *39*, 191–309.
- (33) Tomer, V.; Randall, C. A.; Polizos, G.; Kostelnick, J.; Manias, E. High- and Low-Field Dielectric Characteristics of Dielectrophoretically Aligned Ceramic/Polymer Nanocomposites. *J. Appl. Phys.* **2008**, *103*, 034115.
- (34) Kremer, F.; Schönhals, A. *Broadband Dielectric Spectroscopy*; Springer: Verlag Berlin Heidelberg, 2003.
- (35) Kalmykov, Y. P.; Coffey, W. T.; Crothers, D. S. F.; Titov, S. V. Microscopic Models for Dielectric Relaxation in Disordered Systems. *Phys. Rev. E* **2004**, *70*, 041103.
- (36) Vo, L. T.; Anastasiadis, S. H.; Giannelis, E. P. Dielectric Study of Poly(styrene-co-butadiene) Composites with Carbon Black, Silica, and Nanoclay. *Macromolecules* **2011**, *44*, 6162–6171.
- (37) Yuan, M.; Zhang, G.; Li, B.; Chung, T. C. M.; Rajagopalan, R.; Lanagan, M. T. Thermally Stable Low-Loss Polymer Dielectrics Enabled by Attaching Cross-Linkable Antioxidant to Polypropylene. *ACS Appl. Mater. Interfaces* **2020**, *12*, 14154–14164.
- (38) Li, B.; Yuan, M.; Zhang, S.; Rajagopalan, R.; Lanagan, M. T. Abnormal High Voltage Resistivity of Polyvinylidene Fluoride and Implications for Applications in High Energy Density Film Capacitors. *Appl. Phys. Lett.* **2018**, *113*, 193903.
- (39) Ding, Y.; Pawlus, S.; Sokolov, A. P.; Douglas, J. F.; Karim, A.; Soles, C. L. Dielectric Spectroscopy Investigation of Relaxation in C60–Polysoprene Nanocomposites. *Macromolecules* **2009**, *42*, 3201–3206.
- (40) Brosseau, C.; Achour, M. E. Variable-Temperature Measurements of the Dielectric Relaxation in Carbon Black Loaded Epoxy Composites. *J. Appl. Phys.* **2009**, *105*, 124102.
- (41) Kotsilkova, R.; Fragiadakis, D.; Pissis, P. Reinforcement Effect of Carbon Nanofillers in an Epoxy Resin System: Rheology, Molecular Dynamics, and Mechanical Studies. *J. Polym. Sci. B Polym. Phys.* **2005**, *43*, 522–533.
- (42) Lounev, I. V.; Musin, D. R.; Dimiev, A. M. New Details to Relaxation Dynamics of Dielectric Composite Materials Comprising Longitudinally Opened Carbon Nanotubes. *J. Phys. Chem. C* **2017**, *121*, 22995–23001.
- (43) Belattar, J.; Graça, M. P. F.; Costa, L. C.; Achour, M. E.; Brosseau, C. Electric Modulus-Based Analysis of the Dielectric Relaxation in Carbon Black Loaded Polymer Composites. *J. Appl. Phys.* **2010**, *107*, 124111.
- (44) Dang, Z.-M.; Wu, J.-P.; Xu, H.-P.; Yao, S.-H.; Jiang, M.-J.; Bai, J. Dielectric Properties of Upright Carbon Fiber Filled Poly(vinylidene Fluoride) Composite with Low Percolation Threshold and Weak Temperature Dependence. *Appl. Phys. Lett.* **2007**, *91*, 072912.
- (45) Logakis, E.; Pandis, C.; Peoglos, V.; Pissis, P.; Pionteck, J.; Pötschke, P.; Mičušik, M.; Omastová, M. Electrical/Dielectric Properties and Conduction Mechanism in Melt Processed Polyamide/Multi-Walled Carbon Nanotubes Composites. *Polymer* **2009**, *50*, 5103–5111.

(46) Sidebottom, D. L. Colloquium: Understanding Ion Motion in Disordered Solids from Impedance Spectroscopy Scaling. *Rev. Mod. Phys.* **2009**, *81*, 999–1014.

(47) Yuan, M.; Li, B.; Zhang, S.; Rajagopalan, R.; Lanagan, M. T. High-Field Dielectric Properties of Oriented Poly(vinylidene fluoride-co-hexafluoropropylene): Structure-Dielectric Property Relationship and Implications for Energy Storage Applications. *ACS Appl. Polym. Mater.* **2020**, *2*, 1356–1368.

(48) Li, B.; Sarkarat, M.; Baker, A.; Randall, C. A.; Manias, E. Interfacial Effects on the Dielectric Properties of Elastomer/Carbon-Black/Ceramic Composites. *MRS Adv.* **2021**, *6*, 247–251.

(49) Song, Y.; Noh, T. W.; Lee, S.-I.; Gaines, J. R. Experimental Study of the Three-Dimensional Ac Conductivity and Dielectric Constant of a Conductor-Insulator Composite Near the Percolation Threshold. *Phys. Rev. B* **1986**, *33*, 904–908.

(50) Namikawa, H. Characterization of the Diffusion Process in Oxide Glasses Based on the Correlation between Electric Conduction and Dielectric Relaxation. *J. Non-Cryst. Solids* **1975**, *18*, 173–195.